

Article

## LaNi<sub>0.3</sub>Co<sub>0.7</sub>O<sub>3-δ</sub> and SrFe<sub>0.2</sub>Co<sub>0.8</sub>O<sub>3-δ</sub> Ceramic Materials: Structural and Catalytic Reactivity under CO Stream

Andarair Gomes dos Santos <sup>1</sup>, Madjid Arab <sup>2,\*</sup>, Loic Patout <sup>2</sup> and Carlson Periera de Souza <sup>3</sup>

<sup>1</sup> Universidade Federal Rural do Semi-Árido, DACS, Campus Mossoró-F. Mota, Costa e Silva, 59.625-900, Mossoró/RN, Brazil; E-Mail: andarair@ufersa.edu.br

<sup>2</sup> Université de Toulon, IM2NP, UMR CNRS 7334, Av. de l'Université, Bat R, B. P. 20132, 83957, LA GARDE Cedex, France; E-Mail: patout@univ-tln.fr

<sup>3</sup> Universidade Federal do Rio Grande do Norte, Núcleo Tecnológico, Campus Universitário, L. Nova, 59078-970, Natal/RN, Brazil; E-Mail: carlson@ufrnet.br

\* Author to whom correspondence should be addressed; E-Mail: arab@univ-tln.fr; Tel.: +33-4-9414-2533; Fax: +33-4-9414-2168.

Received: 7 November 2013; in revised form: 20 February 2014 / Accepted: 21 February 2014 / Published: 31 March 2014

---

**Abstract:** In this study, we presented the synthesis of LaNi<sub>0.3</sub>Co<sub>0.7</sub>O<sub>3-δ</sub> (LNCO) and SrCo<sub>0.8</sub>Fe<sub>0.2</sub>O<sub>3-δ</sub> (SFCO) perovskites and their catalytic reactivity under CO gas flow. The synthesis method is based on the complexation method combining ethylenediaminetetraacetic acid (EDTA)-citrate. The as-prepared materials were characterized using X-ray diffraction/Rietveld refinement and electron microscopy. The diffractograms and Rietveld refinement showed that the EDTA-citrate method allows us to obtain monophasic powders with submicronic size. The structural analyses revealed different morphologies linked to the crystallinity of LNCO and SFCO, and to the mean crystallite size. The catalytic performances of LNCO and SFCO were studied *in situ* by Fourier Transform InfraRed spectrometer as a function of time and temperature. The catalytic process gave rise to total oxidation with carbon dioxide and water production. LNCO and SFCO exhibit the same profile for catalytic activity with a conversion rate of twice as high for LNCO. Below 150 °C, the kinetic conversion is slow, but beyond this temperature they reach rapidly the complete transformation at 250 °C and 275 °C for LNCO and SFCO, respectively.

**Keywords:** perovskite; catalytic properties; infrared spectroscopy; CO oxidation.

---

## 1. Introduction

Since its discovery in the 1980s by Teraoka *et al.* [1], perovskite  $\text{SrCo}_{0.8}\text{Fe}_{0.2}\text{O}_{3-\delta}$  has presented itself as an extremely versatile material [2–4]. There is currently still positive speculation about the perovskites including this particular composition. In order to develop materials for specific applications, many authors have used doping elements on the A-site of the  $\text{ABO}_3$  structure with multivalent B-site cations [5], or changed the methodology of synthesis [6,7] to improve their chemical and/or thermal stability. Rajeev *et al.* reported that Lanthanum nickelates and cobaltates with perovskite structure (like  $\text{ABO}_3$ ) can have a mixed electronic and ionic conductivity [7]. The oxygen defect concentration of perovskites is typically tuned by substituting B-site cations with more or less reducible cations or by substituting A-site cations with cations of different charge. For example, increasing substitution of  $\text{Sr}^{2+}$  for  $\text{La}^{3+}$  on the A-site of  $\text{LaFe}_{0.2}\text{Co}_{0.8}\text{O}$  leads to increased oxygen nonstoichiometry and subsequently increased ionic conductivity at the expense of stability of the cubic perovskite phase [8].

Recently, these materials have been used for catalyst or supported media for the production of oxygen from air [9], which justifies its constant research. This fact is attributed to the capacity of this simple structure to accommodate a wide variety of ions with different valences and it can be easily synthesized due to its chemical structure flexibility [10,11], indicating the importance of this type of perovskite oxide. However, only a small fraction of materials presenting perovskite structure has been explored in the catalysis field at low temperature [12–14], although a catalyst is actually used in the majority of the chemical and petrochemical industrial processes. Some perovskites with different compositions were tested as catalysts by Doggali *et al.* [15] and Seyfi *et al.* [16] on carbon monoxide oxidation. According to some authors, perovskites used as catalysts were activated and its stability was reached rapidly, presenting a complete conversion of CO in the temperature range from 220 °C to 355 °C. Other perovskites such as  $\text{LaNi}_{(1-x)}\text{Co}_x\text{O}_{3-\delta}$ , synthesized by the discontinuous precipitation method, have also been tested as catalysts on the conversion of methane to syngas by  $\text{CO}_2$  reforming [13]. Perovskites with the composition  $\text{LaNi}_{0.3}\text{Co}_{0.7}\text{O}_{3-\delta}$  have shown to be more active and also resistant to deactivation after 10 h of reaction.

Therefore, the main purpose of this research work is to synthesize and to characterize the  $\text{LaNi}_{0.3}\text{Co}_{0.7}\text{O}_{3-\delta}$  and  $\text{SrCo}_{0.8}\text{Fe}_{0.2}\text{O}_3$  perovskites' structure and to compare their catalytic properties under carbon monoxide oxidation from room temperature to 300 °C.

## 2. Results and Discussion

### 2.1. Structural Analysis: Electron Microscopy and X-ray Diffraction

Sample morphologies were analyzed by SEM and TEM. For both samples, the grain agglomeration gave rise to different morphologies, as shown in Figure 1a,b. In this case of SFCO, the obtained structure was more compact with heterogeneous grain in the plate shape. Or for LNCO, the sample

was less dense with a pseudo-spherical form and the same grain size (Figure 1c,d). Both samples showed small crystallite size less than 50 nm. In addition, the electron diffraction patterns (inserted figures in Figure 1c,d) reveal the well crystallization of the sample.

The observed porosity is due to the released gases during heat treatment [17,18]. For LNCO, the porosity is mainly observed on the grains boundary; but for SFCO the pores were appeared in the large aggregate due to their large size.

To refine the structural analysis, the XRD characterizations were carried out. Figure 2a,b shows the obtained diffractograms of LNCO and SFCO materials. According to the obtained results, the pure phases were obtained from the adopted synthesis method, which are confirmed and checked by JCPDS factsheets. Both patterns (Figure 1a,b) show the same Bragg angle position with a very good agreement and without any peaks of residual oxide forms (AOx). For LNCO, the structure can be indexed to be a rhombohedral phase according to the ICSD (n: 150874), but for SFCO, the structure is identified as cubic phase with Inorganic Crystal Structures Database ICSD (n: of 79022). These structures are in agreement with those obtained by SAED reported in the literature [19,20] for samples prepared by the conventional high temperature ceramics method.

**Figure 1.** Electron microscopy images of (a,c) for LNCO and (b,d) for SFCO, (c) and (d) correspond to TEM images of elementary grain of the powders. The inserted pictures, in (c) and (d), correspond to the electron diffraction patterns confirming the crystallization structure.

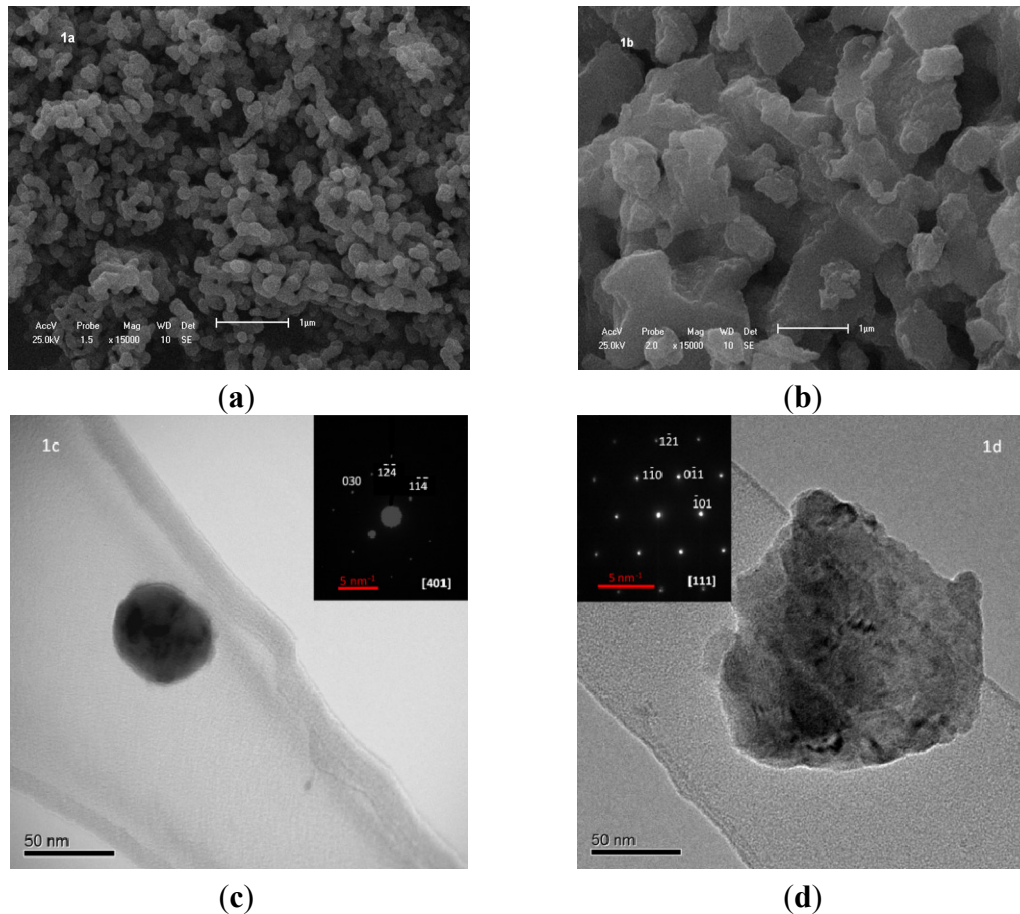


**Figure 2.** XRD patterns for the powder samples of LNCO (a) and SFCO (b). For both samples, pattern 1 corresponds to the experimental measurement data; pattern 2 is calculated by the Rietveld refinement; and the third pattern is the difference of the theoretical and experimental results.

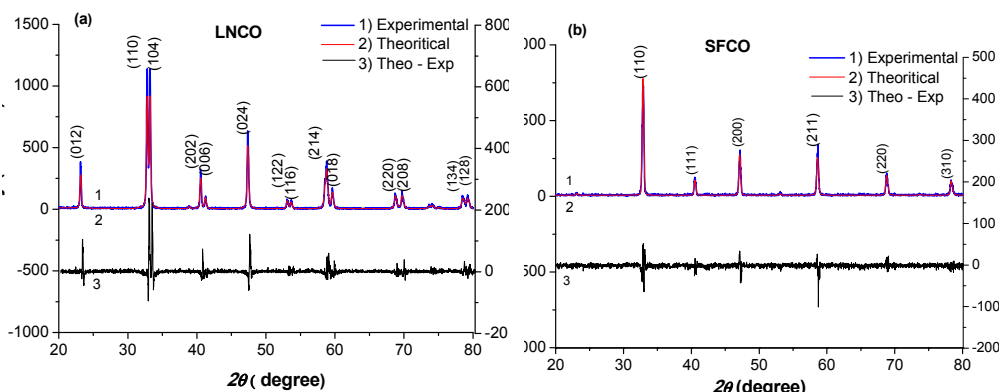


Table 1 shows the crystallographic parameters of the prepared materials obtained from the diffractograms and Rietveld refinement. We observe that the volume of LNCO is five times larger than SFCO but shows a smaller crystallite size; the corresponding particle size is 37 and 45 nm, respectively. However, these values are the same order of magnitude as those obtained by transmission electron microscopy.

**Table 1.** Crystallographic parameters of the samples studied obtained from the diffractograms and from Rietveld refinement.

Samples	$\text{LaNi}_{0.3}\text{Co}_{0.7}\text{O}_{3-\delta}$	$\text{SrCo}_{0.8}\text{Fe}_{0.2}\text{O}_{3-\delta}$
<b>Crystallographic parameters</b>		
Crystal structure	Rhombohedral	Cubic
Lattice parameters (Å)		
a	5.4	3.8
b	5.4	3.8
c	13.2	3.8
$\alpha$	90	90
$\beta$	90	90
$\gamma$	120	90
Volume of cell (Å <sup>3</sup> )	340	58
Density (gr.cm <sup>-3</sup> )	7	5
Mean crystallite size (nm)	37	45
Residual parameter S	1.4	1.2
Rp (%)	13.2	12.8
Rwp (%)	17.3	16.7
Rexp (%)	11.7	11.1

Analysis of network parameters, unit cells and density, presented in Table 1, reveals that the Rietveld refinement results are compatible with those found in the literature [21–23]. From this table,

it can be observed that the EDTA-citrate synthesis method allows us to obtain these perovskite phases with a nanoscale-sized grain.

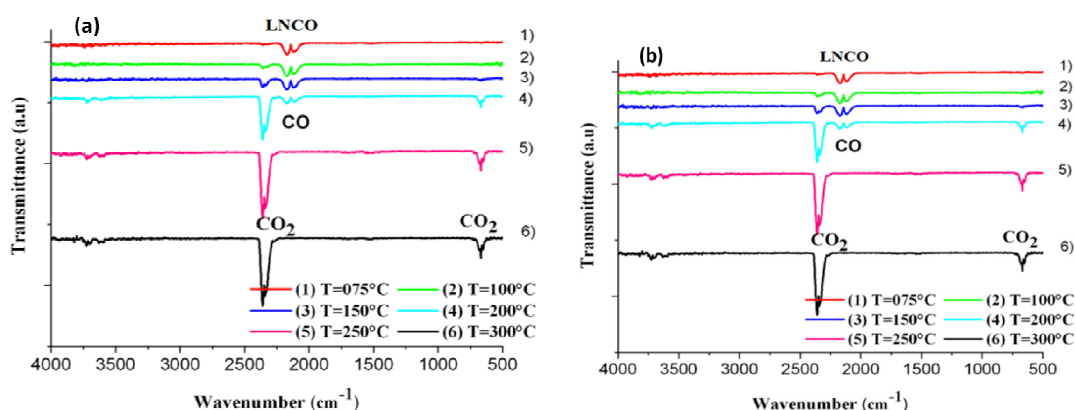
The adjustment obtained by the refinement performed can be confirmed by the value found for the residual parameter  $S$ , which was very close to the unit. Therefore, the values obtained by Rietveld refinement are considered reliable.

The specific surface area measured by the BET method of nitrogen adsorption was found to have the following values: 7 and 5  $\text{m}^2 \text{g}^{-1}$  for LNCO and SFCO, respectively. This specific surface area is obtained after the release of gas produced during the calcination step, which gives rise to different morphologies as indicated previously.

## 2.2. Catalytic Activity

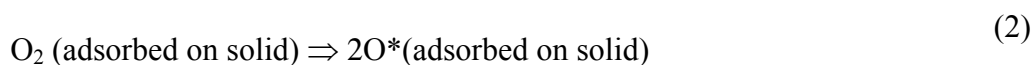
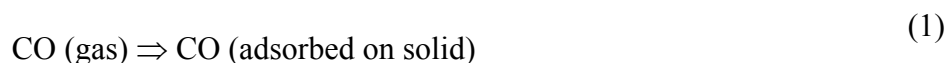
All spectra show the appearance of a new absorption band corresponding to  $\text{CO}_2$ , generated by CO oxidation, as reported in Figure 3. The  $\text{CO}_2$  band intensity increases with the decrease of the CO band as a function of the catalytic temperatures.

**Figure 3.** FTIR spectra analysis of the emitted gases under CO: (a) LNCO and (b) SFCO.



All catalytic phenomena occur through the mechanisms of heterogeneous catalytic reactions involving gas-surface interactions. The conversion of CO to  $\text{CO}_2$  is governed mainly by two mechanisms: the first is related to the recombination of CO with free oxygen adatom after the dissociation of adsorbed dioxygen on the surfaces according to the reaction 3; the second process is thermally activated allowing oxygen vacancies diffusion, conducting to the release of active oxygen required for CO conversion.

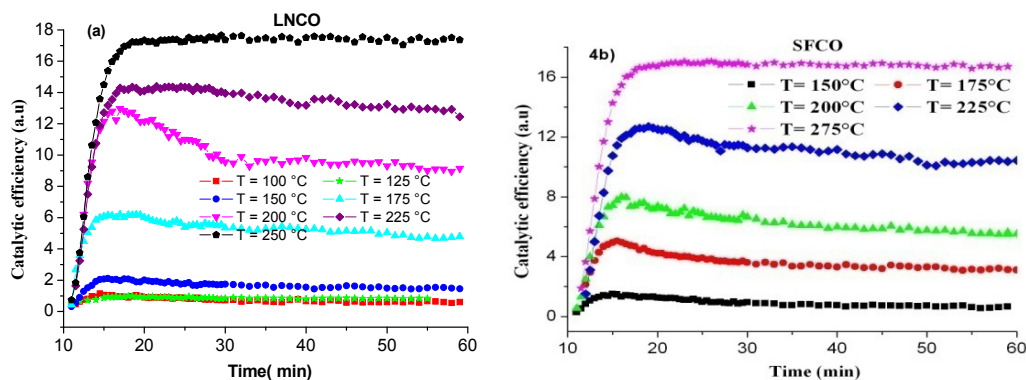
These oxidation mechanisms were derived from the conventional set up Langmuir-Hinshelwood reaction [24]. The reaction at the surface of the ceramic solid should be:



When an oxide material is exposed to air,  $\text{O}_2$  molecules can be adsorbed on the surface and can be ionized into  $\text{O}^{2-}$  or  $\text{O}^-$  by capturing free electrons from materials. This mechanism favors the oxidation reaction according to the reaction 1.

Figure 4a,b show the catalytic activity as a function of exposure time, for LNCO and SFCO respectively. Catalytic efficiency was determined from the measurements of the area under the CO<sub>2</sub> production peak for each spectrum *versus* time exposure to gas.

**Figure 4.** Catalytic activity reported as a function of time at different temperatures: (a) LNCO and (b) SFCO.

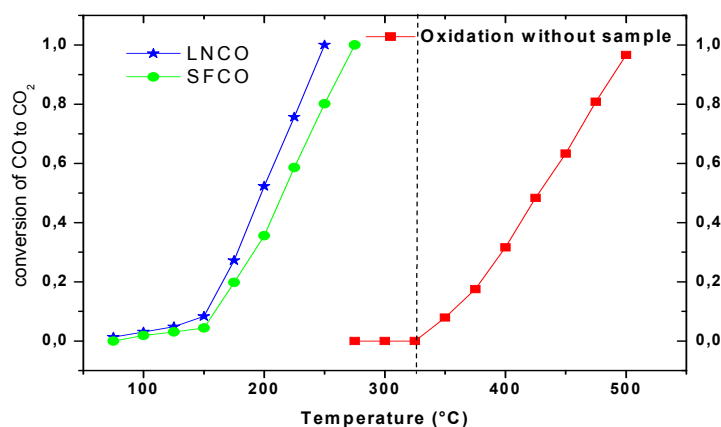


According to Figure 4a,b, catalytic efficiency has the same behavior with a stepped profile, for both samples.

The measurements obtained for temperatures up to 225 °C are characterized by increased efficiency, reaching a maximum value. They are followed by a slight decrease to stabilize on a plateau. The first stage corresponds to the linear increase at the beginning of their action, which corresponds to the total CO transformation. Thus, the maximum point on the curve corresponds to the complete saturation of active sites available on the grain surfaces, corresponding to the optimal ratio of oxygen active site and CO. In a second stage, catalytic efficiency decreases, accompanied by an increase of the CO infrared band intensity. In this case, the smaller amount of oxygen resulted in the trend of decay before the plateau. This behavior can be identified as a reduction process.

Finally, a plateau is reached, whereby the equilibrium was established between the degradation (adsorption) and regeneration (desorption) mechanism. This trend remains stable and unchanged whatever the duration of the experiment as the conditions remain constant.

**Figure 5.** CO oxidation normalized with the specific surface in the presence and lack of catalysts reported as a function of temperature. The profiles are obtained until complete conversion.



To compare the catalysts reactivity, the conversion rates were normalized with respect to the specific surface area, as reported in Figure 5. The samples show the same trend, and exhibit a catalytic activity largely below the temperature of the oxidation without samples, in the gaseous phase. In addition, we observe that LNCO reacts earlier and better than SFCO.

The kinetics conversion becomes significant from 150 °C and increases until the complete CO transformation for both samples. At a fixed temperature, LNCO exhibit a better catalytic efficiency with a conversion rate nearly twice that of SFCO.

Previous studies [25–27] provide evidence of the strong correlation of the catalytic activity (gas conversion) with various parameters: grain size (surface area), temperature and conduction properties. Several studies have been done on CO oxidation of lanthanum nickelates and cobaltates with perovskite structure. Vaz *et al.* [28] reported the incorporation of the cobalt in the perovskite  $\text{LaNiO}_3$  (LNO) by co-precipitation precursor technique giving rise to particles with large size dispersion.

LNO and LCO have a catalytic conversion activity in the temperature range of 100 to 350 °C. For LNCO, the catalytic behavior starts at the same temperature as LCO and reaches the complete conversion more rapidly than LNO, but this trend remains close to that of LCO. The above catalytic evolution is attributed to the substitution of the Co by Ni and the induced change in the crystal structure. Nevertheless, regarding to the catalytic activity produced at T50 and T95, we observe respectively a positive shift of 50 °C and 25 °C of our results than those reported by Vaz *et al.* This can be attributed to the morphology grain (Figure 1) linked to the used synthesis method and the measurement system.

In the literature, several studies have shown a correlation between catalytic activity and the electronic properties of the transition metal ions. The used materials exhibit a thermally activated behavior, which the conductivity increases with increasing temperature in the low temperature range [29]. A bibliographic data showed a correlation between catalytic activity and the electronic configuration in the transition metal [30]. In the case of ferrites, the electronic and ionic conductivity were enhanced by the presence of Co which increase the concentration of mobile oxygen vacancies sites. These sites are mainly located around Ni/Co and Fe/Co cations. The substitution of Co by Ni(Fe) can be explained by slight changes taking place in the structure.

The best catalytic efficiency of LNCO is due to the free oxygen ions ( $\text{O}^{2-}$  or  $\text{O}^-$ ) available on the surface, and favored by the electrons released during the conduction process. This behavior is in agreement with the small polaron hopping mechanism, which suggests the high electron conduction in perovskite-type ferrites takes place through the change of oxidation state of Co, Fe, Ni; from +IV to +III [31]. Thus, the difference of the ionic radius and the substitution of the A and B sites cations promote the generation vacancies, which allow the diffusion of the oxide ions. Teraoka *et al.* reported that higher Co content is an advantage for the diffusion because  $\text{Co}^{3+}$  has a smaller ionic radius as well as smaller energy bending than  $\text{Fe}^{3+}$  [1]. As indicated in the introduction, the best conduction properties of LNCO oxide confirm a higher catalytic activity than SFCO, due to the electronic contribution in the oxidation mechanism.

After a long storage period, structural properties remain identical as to before. For catalytic studies, a heat treatment of around 400 °C is sufficient for gases desorption(water) to recover the same catalytic properties and with the same efficiencies.

### 3. Methodology

#### 3.1. Synthesis Method

Material synthesis was performed based on the complexation method combining EDTA-citrate [32–34]. For materials synthesis, we used ethylenediaminetetraacetic acid (Sigma-Aldrich, St. Louis, MO, USA; 99%), ammonium hydroxide (Sigma-Aldrich, St. Louis, MO, USA; 25%), citric acid (Sigma-Aldrich, St. Louis, MO, USA; 99%), nickel nitrate hexahydrate (Sigma-Aldrich, 98%), strontium nitrate (Sigma-Aldrich, St. Louis, MO, USA; 99%), iron III nitrate nonahydrate (Sigma-Aldrich, St. Louis, MO, USA; 98%), cobalt II nitrate hexahydrate (Sigma-Aldrich, St. Louis, MO, USA; 98%) and deionized water.

The synthesis method consisted of the following: (1) an appropriate amount of acid EDTA was diluted in ammonium hydroxide at a ratio of 1 g:10 mL, and kept under agitation and heating (30–40 °C) until a limpid solution was obtained (solution 1); (2) next, the element-based solution (La, Ni and Co or Sr, Co and Fe) was added at stoichiometrically defined proportions; (3) finally, citric acid was added and the temperature was controlled at around 80 °C until gel formation. A molar ratio of acid EDTA, citric acid and total metal ions of 1:1.5:1 was added to obtain the perovskite-type ceramic material [35]. If precipitation occurred, the pH of the solution was corrected with the addition of 25% NH<sub>4</sub>OH. After gel formation, the samples were submitted to thermal treatment at 800 °C and 950 °C during 300 min, with heating rate of 10 °C/min and 2 °C/min, respectively, for LNCO and SFCO.

#### 3.2. Characterization

The morphologies and diffraction analysis were investigated using a scanning electron microscope SEM (Philips XL 30) and transmission electron microscope TEM with a Scanning area electron diffraction SAED (FEI Tecnai G2, operating at 200 kV) to check the crystallinity.

To identify the expected phases of the powder, X-ray diffraction patterns were recorded on a XRD, Siemens X-ray diffractometer (Shimadzu XRD-6000) working in a  $\theta$ - $\theta$  mode, with a copper X-ray source ( $\lambda(K\alpha_1) = 1.5406 \text{ \AA}$ ). XRD diffractograms were collected from 20° to 80° 2 $\theta$  degrees with a step-by-step scan of 0.02 at a room temperature and then they were compared with Joint Committee on Powder Standards (JCPDS). After obtaining the diffractograms, we used Rietveld refinement to determine the crystallite size of the materials, based on the diffraction peaks of the planes and the Scherrer relation [36–38].

The Rietveld method is used to analyze the refinement of crystalline structures in which all the contributing factors for the intensities measured can be simultaneously refined until the difference between the experimental samples is calculated and minimized [38,39]. The DBWS TOOLS 2.16 program uses the Newton-Raphson algorithm to refine and quantify the intensities measured. Diffractogram peak adjustment is done with the profile of the modified Pseudo-Voigt function containing the mixtures of Lorentzian and Gaussian contributions.

The full width at half maximum (FWHM), extracted from the diffractogram, is used to calculate the size of crystallites and the parameters of the crystalline structure of each phase. The mean size of crystallite is calculated using the Scherrer model [40]. The instrumental correction of full width at half

maximum is calculated with the FWHM of the experimental sample and standard sample of LaB<sub>6</sub> “standard reference material” [41].

### 3.3. Catalytic Activity

The catalytic properties of the samples under a gas mixture (air–CO) in a catalytic reactor were studied *in situ* by Fourier Transformed InfraRed Spectroscopy FTIR (Unicam-Mattson-RS, Cambridge, UK). The catalytic reactor is composed of a stainless steel tube that contains the calcined sample in the form of powder (150 mg) between two porous separators and inert to gases. The reactor is connected to a platform that controls gas composition at the reactor inlet (2500 ppm of CO in air).

The gas flows first through the separator and then crosses the sample at a fixed rate of 10 mL/min. Reactor outlet gas transformed or not by the catalytic action of the sample, is sent to an infrared spectrophotometer working with cube corner technology [42].

Before each measurement, the samples are treated at high temperature (up to 500 °C) under air for 3 h. Blank experiment using neutral atmosphere and reactor cell without sample was carried out. The results are presented under the form of infrared spectra and measured every 30 s for one hour. The intensities of CO and CO<sub>2</sub> absorption bands (peaks surfaces) are used to determine catalytic efficiencies as a function of time and temperature.

These spectra show the emergence of a new absorbance band corresponding to CO<sub>2</sub> generated by CO transformation, according to the following equation:



Where O\* corresponds to the free oxygen on surface linked to the active site.

The intensity variation of CO<sub>2</sub> bands were used to determine the catalytic efficiency evolutions as a function of time and temperature. All measurements were verified several times to check the reproducibility and the stability of the samples.

## 4. Conclusions

The EDTA-citrate method allowed us to obtain monophasic crystallized powders according to the microscopy and diffraction analyzes. The sample morphologies revealed an agglomeration grain with different porosity. The structural analysis obtained from the diffractograms, Rietveld refinement and TEM shown a mean crystallite size of less than 50 nm (37 nm and 45 nm, respectively for LNCO and SFCO).

At the beginning of the catalytic process (around 100 °C), both samples exhibited the same profile in terms of catalytic efficiency and slow conversion kinetics for temperatures below 150 °C. However, at higher temperature, the LNCO sample showed a higher conversion rate of CO than SFCO, which varies until 20% for each used temperature. This difference is linked to the nature of A and B site cations and their radius size on the possible oxygen conduction. Thus, new experiments are planned to investigate the interactions of as-prepared BCO catalyst with CO gas in air–CO mixtures.

## Acknowledgments

To CNPq/CTENEG/CTPETRO for financial support, to UFRN/PPGEQ/LTR for making study facilities available, to NEPGN for providing XRD equipment. We gratefully acknowledge the Provence-Alpes-Cote d'Azur Regional Council, CG83 and TPM for financial support.

## Conflicts of Interest

The authors declare no conflict of interest.

## References

1. Teraoka, Y.; Zhang, H.-M.; Furukawa, S.; Yamazoi, N. Oxygen permeation through perovskite-type oxides. *Chem. Lett.* **1985**, *14*, 1743–1746.
2. Lu, H.; Cong, Y.; Yang, W.S. Oxygen permeability and stability of  $\text{Ba}_{0.5}\text{Sr}_{0.5}\text{Co}_{0.8}\text{Fe}_{0.2}\text{O}_{3-\delta}$  as an oxygen-permeable membrane at high pressures. *Solid State Ionics* **2006**, *177*, 595–600.
3. Fagg, D.P.; Shaula, A.L.; Kharton, V.V.; Frade, J.R. High oxygen permeability in fluorite-type  $\text{Ce}_{0.8}\text{Pr}_{0.2}\text{O}_{2-\delta}$  via the use of sintering aids. *J. Membrane Sci.* **2007**, *299*, 1–7.
4. Cheng, Y.S.; Pena, M.A.; Yeung, K.L. Hydrogen production from partial oxidation of methane in a membrane reactor. *J. Taiwan Inst. Chem. Eng.* **2009**, *40*, 281–288.
5. Chen, W.; Chen, C.-H.; Chen, L.W.; Chen, C.; Winnubst, L. Ta-doped  $\text{SrCo}_{0.8}\text{Fe}_{0.2}\text{O}_{3-\delta}$  membranes: Phase stability and oxygen permeation in  $\text{CO}_2$  atmosphere. *Solid State Ionics* **2011**, *11*, 30–33.
6. Rui, Z.; Ding, J.; Li, Y.; Lin, S.  $\text{SrCo}_{0.8}\text{Fe}_{0.2}\text{O}_{3-\delta}$  sorbent for high-temperature production of oxygen-enriched carbon dioxide stream. *Fuel* **2010**, *89*, 1429–1434.
7. Rajeev, K.P.; Raychaudhuri, A.K. Quantum corrections to the conductivity in a perovskite oxide: A low-temperature study of  $\text{LaNi}_{1-x}\text{Co}_x\text{O}_3$  ( $0 \leq x \leq 0.75$ ). *Phys. Rev. B* **1992**, *46*, 1309–1320.
8. Ahmad, A.L.; Sani, N.A.A.; Zein, S.H.S. Synthesis of a  $\text{TiO}_2$  ceramic membrane containing  $\text{SrCo}_{0.8}\text{Fe}_{0.2}\text{O}_3$  by the sol-gel method with a wet impregnation process for  $\text{O}_2$  and  $\text{N}_2$  permeation. *Ceram. Int.* **2011**, *37*, 2981–2989.
9. Prado, F.; Grunbaum, N.; Caneiro, A.; Manthiram, A. Effect of  $\text{La}^{3+}$  doping on the perovskite-to-brownmillerite transformation in  $\text{Sr}_{1-x}\text{La}_x\text{Co}_{0.8}\text{Fe}_{0.2}\text{O}_{3-\delta}$  ( $0 \leq x \leq 0.4$ ). *Solid State Ionics* **2004**, *167*, 147–154.
10. Chang, L.; Sasirekha, N.; Rajesh, B.; Chen, Y. CO oxidation on ceria- and manganese oxide-supported gold catalysts. *Sep. Purif. Technol.* **2007**, *58*, 211–218.
11. Soares, A.B.; Silva, P.R.N.; Freitas, J.C.C.; Almeida, C.M. Estudo da oxidação total do etanol usando óxidos tipo perovskita (B = Mn, Ni, Fe). *Química Nova* **2007**, *30*, 1061–1066.
12. Lima, S.M.; Assaf, J.M. Síntese e caracterização de perovskitas  $\text{LaNi}_{1-x}\text{Co}_x\text{O}_3$  como precursores de catalisadores para a conversão do metano a gás de síntese pela reforma com  $\text{CO}_2$ . *Química Nova* **2007**, *30*, 298–303.
13. Worayingyong, A.; Kangvansura, P.; Ausadasuk, S.; Praserttham, P. The effect of preparation: Pechini and Schiff base methods, on adsorbed oxygen of  $\text{LaCoO}_3$  perovskite oxidation catalysts. *Colloids Surfaces A* **2008**, *315*, 217–225.

14. Stathopoulos, V.N.; Belessi, V.C.; Bakas, T.V.; Neophytides, S.G.; Costa, C.N.; Pomonis, P.J.; Efstathiou, A.M. Comparative study of La-Sr-Fe-O perovskite-type oxides prepared by ceramic and surfactant methods over the CH<sub>4</sub> and H<sub>2</sub> Lean-de NO<sub>x</sub>. *Appl. Catal.* **2009**, *93*, 1–11.
15. Doggali, P.; Kusaba, S.; Teraoka, Y.; Chankapure, P.; Rayalu, S.; Labhsetwar, N. La<sub>0.9</sub>Ba<sub>0.1</sub>CoO<sub>3</sub> perovskite type catalysts for the control of CO and PM emissions. *Catal. Commun.* **2010**, *11*, 665–669.
16. Seyfi, B.; Baghalha, M.; Kazemian, H. Modified LaCoO<sub>3</sub> nano-perovskite catalysts for the environmental application of automotive CO oxidation. *Chem. Eng. J.* **2009**, *148*, 306–311.
17. Dreyer, C.; Samanos, B.; Vogt, F. Coke calcination levels and aluminum anode quality. *Light Metals (Warrendale)* **1996**, *4*, 535–542.
18. Garbarino, R.M.; Tonti, R.T. Desulfurization and its effect on calcined cokeproperties. *Light Metals (Warrendale)* **1993**, *4*, 517–520.
19. Harrison, W.T.A.; Lee, T.H.; Yang, Y.L.; Scarfe, D.P.; Liu, L.M.; Jacobson, A.J. Aneutron diffraction study of two strontium cobalt iron oxides. *Mater. Res. Bull.* **1995**, *30*, 621–630.
20. Liu, L.M.; Lee, T.H.; Yang, Y.L.; Jacobson, A.J. A thermogravimetric study of the phase diagram of strontium cobalt iron oxide, SrCo<sub>0.8</sub>Fe<sub>0.2</sub>O<sub>3-δ</sub>. *Mater. Res. Bull.* **1996**, *31*, 29–35.
21. Qiu, L.; Lee, T.H.; Liu, L.M.; Yang, Y.L.; Jacobson, A.J. Oxygen permeation studies of SrCo<sub>0.8</sub>Fe<sub>0.2</sub>O<sub>3</sub>. *Solid State Ionics* **1995**, *76*, 321–329.
22. Gopalakrishnan, J.; Colsmann, G.; Reute, B. A Study of LaNi<sub>1-x</sub>Co<sub>x</sub>O<sub>3</sub> System. *Z. Anorg. Allg. Chem.* **1976**, *424*, 155–161.
23. McIntosh, S.; Vente, J.F.; Haije, W.G.; Blank, D.H.A.; Bouwmeester, H.J.M. Structure and oxygen stoichiometry of SrCo<sub>0.8</sub>Fe<sub>0.2</sub>O<sub>3-δ</sub> and Ba<sub>0.5</sub>Sr<sub>0.5</sub>Co<sub>0.8</sub>Fe<sub>0.2</sub>O<sub>3-δ</sub>. *Solid State Ionics* **2006**, *177*, 1737–1742.
24. Ertl, G.; Engel, T. Elementary steps in the catalytic oxidation of carbon monoxide on platinum metals. *Adv. Catal.* **1979**, *28*, 1–78.
25. Nowakowski, P.; Dallas, J.P.; Villain, S.; Kopia, A.; Gavarrri, J.R. Structure, microstructure, and size dependent catalytic properties of nanostructured ruthenium dioxide. *J. Solid State Chem.* **2008**, *181*, 1005–1016.
26. Voorhoeve, R.J.H.; Remeika, J.P.; Gallagher, P.K. Perovskite oxides: Materials science in catalysis. *Science* **1977**, *195*, 827–833.
27. Tascon, J.M.D.; Tejuca, L.G. Catalytic activity of perovskite-type oxides LaMeO<sub>3</sub>. *React. Kinet. Catal. Lett.* **1980**, *15*, 185–191.
28. Vaz, T.; Salker, A.V. Preparation, characterization and catalytic CO oxidation studies on LaNi<sub>1-x</sub>Co<sub>x</sub>O<sub>3</sub> system. *Mater. Sci. Eng. B* **2007**, *143*, 81–84.
29. Ren, Y.; Küngas, R.; Gorte, R.J.; Deng, C. The effect of A-site cation (Ln = La, Pr, Sm) on the crystal structure, conductivity and oxygen reduction properties of Sr-doped ferrite perovskites. *Solid State Ionics* **2012**, *212*, 47–54.
30. Voorhoeve, R.J.H. *Advance Materials in Catalysis*; Plenum Press: New York, NJ, USA, 1975; Chapter 5.
31. Montini, T.; Bevilacqua, M.; Fonda, E.; Casula, M.F.; Lee, S.; Tavagnacco, C.; Gorte, R.J.; Fornasiero, P. Relationship between electrical behavior and structural characterization in Sr-doped LaNi<sub>0.6</sub>Fe<sub>0.4</sub>O<sub>3-δ</sub> mixed oxides. *Chem. Mater.* **2009**, *21*, 1768–1774.

32. Shao, Z.; Dong, H.; Xiong, G.; Cong, Y.; Yang, W. Performance of a mixed-conducting ceramic membrane reactor with high oxygen permeability for methane conversion. *J. Membrane Sci.* **2001**, *183*, 181–192.
33. Ghadimi, A.; Alaei, M.A.; Behrouzifar, A.; Asadi, A.A.; Mohammadi, T. Oxygen permeation of  $\text{Ba}_x\text{Sr}_{1-x}\text{Co}_{0.8}\text{Fe}_{0.2}\text{O}_{3-\delta}$  perovskite-type membrane: Experimental and modeling. *Desalination* **2011**, *270*, 64–75.
34. Ikeguchi, M.; Yoshino, Y.; Kanie, K.; Nomura, M.; Kikuchi, E.; Matsukata, M. Effects of preparation method on oxygen permeation properties of  $\text{SrFeCo}_{0.5}\text{O}_x$  membrane. *Sep. Purif. Technol.* **2003**, *32*, 313–318.
35. Lopes, F.W.B.; Arab, M.; Macedo, H.P.; de Souza, C.P.; de Souza, J.F.; Gavarri, J.R. High temperature conduction and methane conversion capability of  $\text{BaCeO}_3$  perovskite. *Powder Technol.* **2012**, *219*, 186–192.
36. Azároff, L.V. *Elements of X-ray Crystallography*; McGraw-Hill Book Company: New York, NY, USA, 1968.
37. Young, R.A. *The Rietveld Method, International Union of Crystallography (IUCr)*; Oxford University Press Inc.: New York, NY, USA, 1995.
38. Jenkins, R.; Synder, L. *Introduction to X-ray Powder Diffractometry*; Wiley-Interscience: New York, NY, USA, 1996.
39. Gualtieri, M.L.; Prudenziati, M.; Gualtieri, A.F. Quantitative determination of the amorphous phase in plasma sprayed alumina coatings using the rietveld method. *Surface Coatings Technol.* **2006**, *201*, 2984–2989.
40. Martinez, J.R.; Palomares-Sánchez, S.; Ortega-Zarzosa, G.; Ruiz, F.; Chumakov, Y. Rietveld refinement of amorphous  $\text{SiO}_2$  prepared via sol-gel method. *Mater. Lett.* **2006**, *60*, 3526–3529.
41. Rasberry, S.; Hubbard, C.; Zhang, Y.; McKenzie, R. *Certificate of Analysis, Standard Reference Material 660. Instrument Line Position and Profile Shape Standard for X-ray Powder Diffraction*; National Institute of Standards Technology Center for Neutron Research: St Louis, MO, USA, 1989.
42. David, M.; Arab, M.; Guinneton, F.; Flahaut, E.; Bakiz, B.; Nowakowski, P.; Gavarri, J.R. Electrical properties and reactivity under air–CO flows of composite systems based on ceria coated carbon nanotubes. *Chem. Eng. J.* **2011**, *171*, 272–278.